Alexandria Engineering Journal (2010) 49, 339–348

Alexandria University

Alexandria Engineering Journal

www.elsevier.com/locate/aej
www.sciencedirect.com

ORIGINAL ARTICLE

Structural behavior of architectural glass plates

Mostafa M. El-Shami [a,b,*], Yasser E. Ibrahim [c], Mohsen Shuaib [a]

[a] Department of Civil Engineering, Faculty of Engineering, Menoufia University, Egypt
[b] Department of Civil and Environmental Engineering, Texas Tech University, USA
[c] Department of Structural Engineering, Faculty of Engineering, Zagazig University, Egypt

Received 22 February 2010; accepted 14 July 2010
Available online 26 January 2011

KEYWORDS
Finite element;
Architectural glass;
Plates;
Mindlin plate theory

Abstract Architectural designers frequently use glass plates that have shapes other than rectangular in both residential and commercial buildings. Commonly, one sees glass plates with trapezoidal, triangular, hexagonal, and circular shapes. For example; window glass in aircraft control tower cabs leans outward to enable ground controllers to have a good view of operations. Consequently, aircraft control tower cabs have glass plates that have trapezoidal shapes. This paper deals with the structural behavior of glass plates other than rectangular shapes. A higher order finite element model based upon Mindlin plate theory was employed to analyze different shapes of glass plates. First, a comparison between experimental and finite element results for a tested trapezoidal glass plate is presented, which shows a very good agreement. Then, the finite element model was used to compare load-induced stresses with those for bounding rectangular shapes. Results of analysis are presented and discussed.

1. Introduction

Designers of architectural glazing use nonrectangular glass plates, and therefore considerable interest has been generated within the glazing design community. Architects and engineers are encountering difficulty with glass design processes for shapes other than rectangular. This difficulty arises from two reasons: (a) an inability to perform nonlinear analysis on glass plates with large deflection and (b) an inability to perform failure predication analysis. A thin glass plate might undergo deflection up to 10 times its thickness before fracture. Of course the linear plate theory is no longer applicable to this analysis because of the development of membrane stresses in addition to bending stresses. Many researchers have contributed to nonlinear analysis of glass plates. The research is classified into two categories, theoretical investigations and

* Corresponding author at: Civil Engineering Department, Menoufia University, Egypt.
E-mail addresses: mostafa.el-shami@ttu.edu (M.M. El-Shami), yibrahim@vt.edu (Y.E. Ibrahim), mf-shuaib@hotmail.com (M. Shuaib).

Peer review under responsibility of Faculty of Engineering, Alexandria University.
doi:10.1016/j.aej.2010.07.001

Production and hosting by Elsevier

experimental testing. The Glass Research and Testing Laboratory (GRTL) at Texas Tech University (TTU) has made substantial contributions to this subject.

Kaiser [7] solved a square plate using a finite difference technique. His model was limited to a maximum lateral displacement of 2.5 times the plate thickness. Levy [8] conducted a formulation for nonlinear analysis of simply supported plates with zero in plane reaction at the edge, which is not suitable for glass plates. Pilkington [11] compared monolithic glass strength to the strength of laminated glass (LG) plate specimens made with sheet and float glass. This comparison was for rectangular shapes only. Beason [2] presented an analytical model using von Karman [15] equations and Galerkin method technique to calculate the strength of glass plates. Vallabhan [12] actually formulated the model and developed a finite difference model for rectangular glass plates which is relatively efficient when compared to that of previous investigators.

Vallabhan et al. [13] developed a mathematical model for LG plates based on the finite difference method. The comparison of results with the experimental ones was fairly good, but the mathematical model needed improvement. El-Shami et al. [6] developed a new finite element model for nonlinear analysis of monolithic rectangular glass plates that is capable of handling thin or thick plates. Norville et al. [9] presented a discussion concerning the behavior and strength of LG beams. They also observed that monolithic glass having the same thickness as LG does not necessarily provide an upper bound for LG strength. Vallabhan and El-Shami [14] improved the model of El-Shami et al. [6] to handle shapes other than rectangular, especially trapezoidal glass plates. Recently, El-Shami and Norville [5] developed a sophisticated finite element model for LG plates.

In this paper, nonlinear finite element models (FEM) are employed for both monolithic and laminated glass (LG) plates. Experimental results of tests which were conducted at the Glass Research and Testing Laboratory (GRTL) at Texas Tech University for monolithic and LG trapezoidal glass plates are compared with the FEM results. Then the FEM is applied for glass plates with triangular, hexagonal and circular shapes. Finally the results are discussed and the conclusion is drawn.

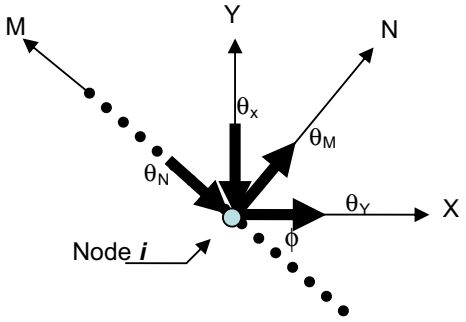

Figure 1 Boundary conditions for inclined side.

2. Finite element model

Since lateral deflections of the panels are large compared to their thickness, nonlinear plate theory is necessary in the analysis. The analysis is based upon Mindlin plate theory using von Karman's [15] assumption. The finite element models for monolithic and LG plates have been mentioned in the previous publications [5,6,14]; however, they are listed here for completeness only. For a monolithic plate, the element has 9 nodes with 5 degrees of freedom for each node. The displacements and rotations are:

$$u = \sum_{i=1}^{9} N_i(\xi,\eta)u_i, \quad v = \sum_{i=1}^{9} N_i(\xi,\eta)v_i, \quad w = \sum_{i=1}^{9} N_i(\xi,\eta)w_i$$
$$\theta_x = \sum_{i=1}^{9} N_i(\xi,\eta)\theta_{xi}, \quad \theta_y = \sum_{i=1}^{9} N_i(\xi,\eta)\theta_{yi} \tag{1}$$

where $N_i,\ i = 1,\ldots,9$ are the shape functions [16]. The total nonlinear stiffness matrix $[K_l]$ is calculated as [3]:

$$[K_l] = \int_V [B_l]^T[D][B_0] + [B_0]^T[D][B_l] + [B_l]^T[D][B_l]\,dV \tag{2}$$

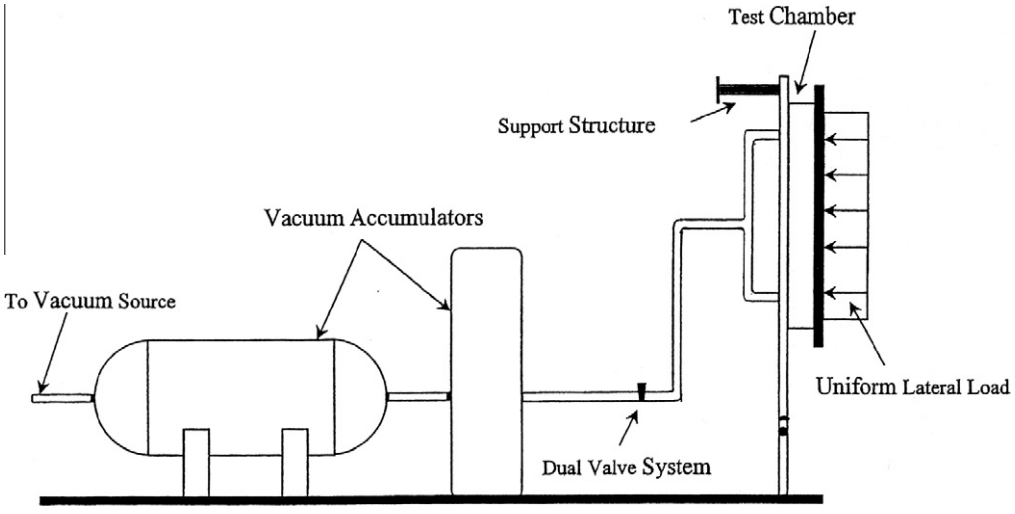

Figure 2 Test setup facility.

where $[B_l]$ denotes the relationship between nonlinear strains and displacements vector, $[B_0]$ denotes the relationship between linear strains and displacements vector, and $[D]$ denotes the elasticity matrix. The final stiffness matrix is given as:

$$[K_T] = [K_0] + [K_l] + [K_\sigma] \tag{3}$$

where $[K_0]$ and $[K_\sigma]$ are linear stiffness matrix and initial stress matrix, respectively [16].

For LG, a common thin elastomeric interlayer called polyvinyl butyral (PVB) is used to bond two or more thin glass plates to form a composite. The effect of the interlayer material is taken as shear strain. The element here is the same as that used in the monolithic plate model; however, there is an upper plate element and a lower plate element. The two plates share the same bending displacements, but each plate has its own membrane displacements. Thus, the total number of degrees of freedom will be 7 per node. The stiffness matrix due to the interlayer material [5] is given as:

$$[K_{INT}] = \frac{G_{INT}}{h}[B]^t[I][B]dx\,dy \tag{4}$$

where $[B]$ denotes the relationship between the shear strain and the displacement vector, and G_{INT} denotes the modulus of rigidity for the interlayer. Stiffness matrix for the whole composite is given as [5]:

$$[\overline{K}_T] = [K_p] + [K_{INT}] \tag{5}$$

in which, $[K_p]$ is the total stiffness matrix for the upper and lower plates.

For both FEM models, the methodology consists of tangent element stiffness matrix with an incremental procedure to analyze the plate. The boundary condition is simply plate supported at all sides. For inclined sides with angle ϕ (see Fig. 1) such as trapezoidal and triangular plates, the rotation normal to the side will be [4]:

$$\alpha\theta_X + \beta\theta_Y = \theta_M \tag{6}$$

where

$$\alpha = \sin\phi, \quad \beta = \cos\phi$$

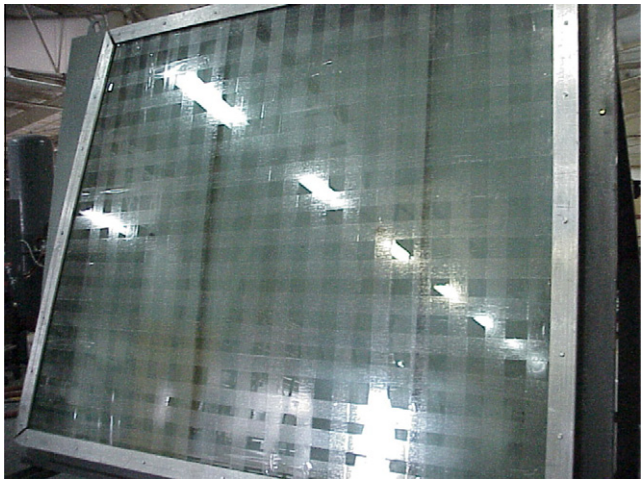

Figure 3 Test chamber.

θ_X, θ_Y and θ_M are the rotations about X, Y and M axes, respectively.

In the penalty approach [3], the total potential energy function is augmented by the strain energy of a fictitious spring with a very large spring constant C in the direction of the prescribed displacement. So the total potential energy function (Π_M) can be written as:

$$\Pi_M = \frac{1}{2}\{u\}^t[K]\{u\} + \frac{1}{2}C\nabla^2 + V \tag{7}$$

where $\{u\}$ denotes the displacement vector, $[K]$ denotes the global stiffness matrix, V denotes the potential energy, and ∇ is the prescribed condition such as:

$$\nabla = \alpha\theta_X + \beta\theta_Y - \theta_M \approx 0 \tag{8}$$

Differentiating Π_M with respect to both θ_X and θ_Y, we get the necessary coefficients of the global stiffness matrix at the prescribed node i. The only change in the global stiffness matrix will be with the terms associated with θ_X and θ_Y as following:

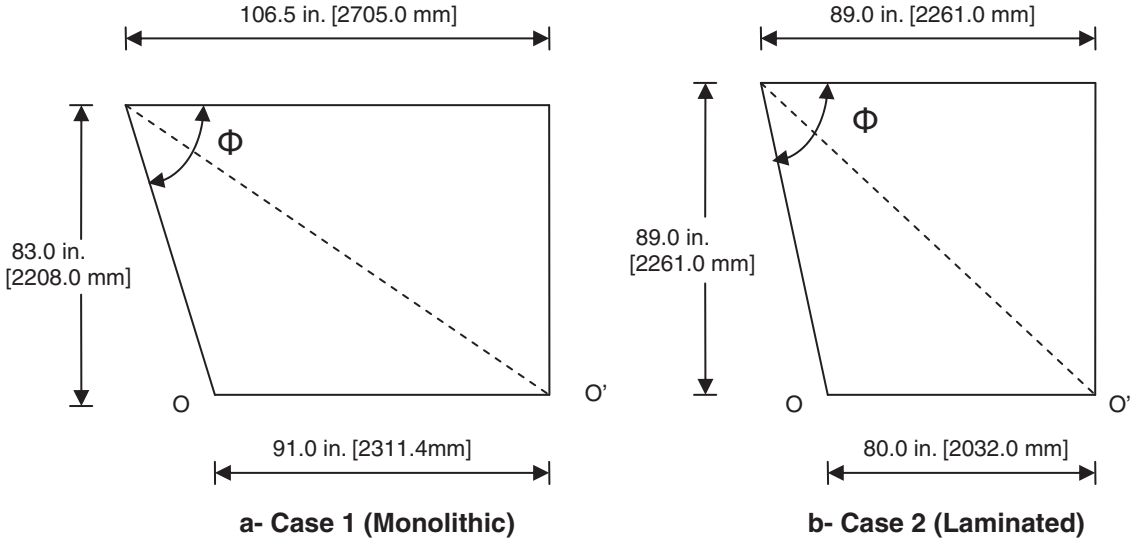

Figure 4 Dimension of test specimens.

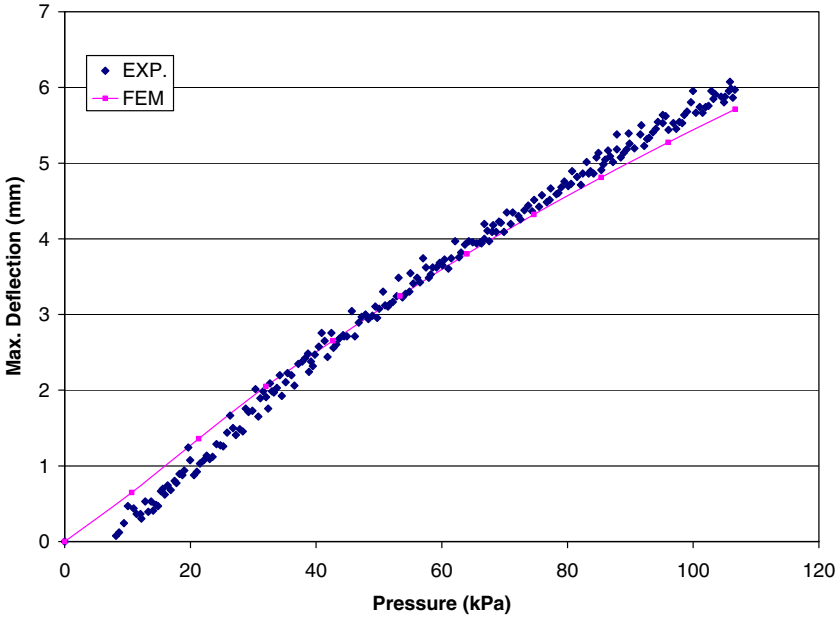

Figure 5 Maximum lateral displacements versus pressure.

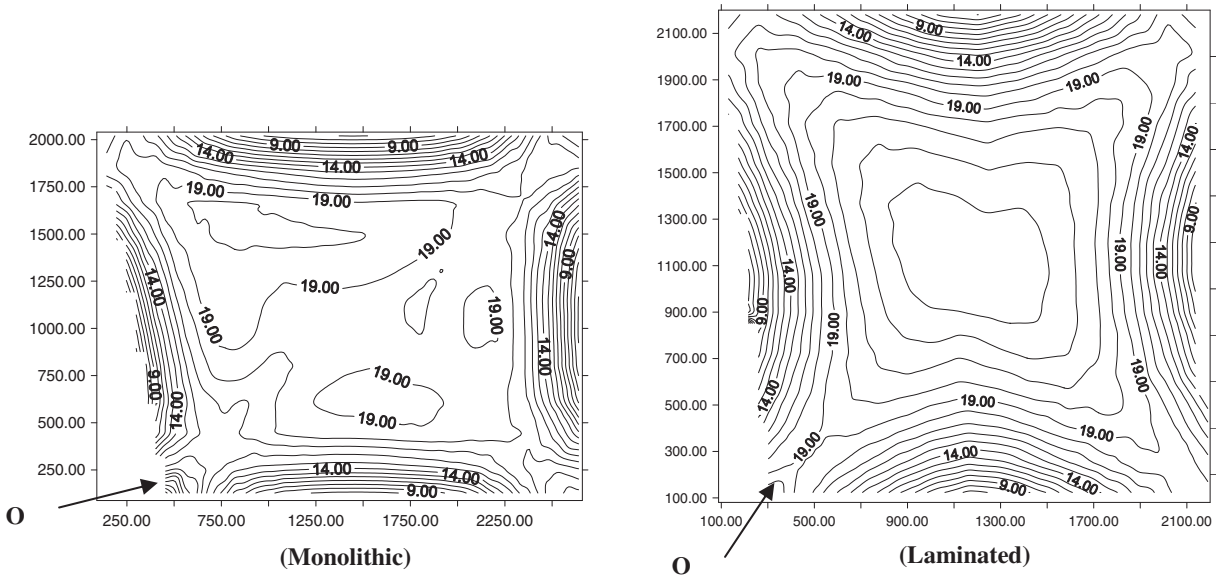

Figure 6 Maximum tensile principal stresses (trapezoidal shape) (stress contours in MPa; dimensions on axes in mm).

$$\begin{bmatrix} \vdots & \vdots & \\ \cdots & K_{5i-4,5i-4}+C\alpha^2 & K_{5i-4,5i}+C\alpha\beta & \cdots \\ \cdots & K_{5i,5i-4}+C\alpha\beta & K_{5i,5i}+C\beta^2 & \cdots \\ & \vdots & \vdots & \end{bmatrix} \tag{9}$$

where $5i-4$ and $5i$ are the order of θ_X and θ_Y associated with node i.

3. Experimental and numerical examples

The GRTL staff at Texas Tech University developed the testing facilities which were used to test 34 specimens. All the specimens were supplied by the Federal Aviation Administration (FAA). Test series FAA 1 (Case 1) consisted of 13 monolithic annealed insulated glazed (IG) units that had undergone approximately 21 years of in-service life. Test series FAA 2 (Case 2) consisted of LG units that had undergone in-service life of less than 6 months. Both of the two series samples were used as large trapezoidal window glass at aircraft control towers in the United States. The testing facility and testing procedure used in this research were similar to those used in previous GRTL studies which include a test chamber and support structure, a vacuum accumulation system, and a data collection system (see Fig. 2). Two different test chambers, designed specifically for the specimens it would hold (see

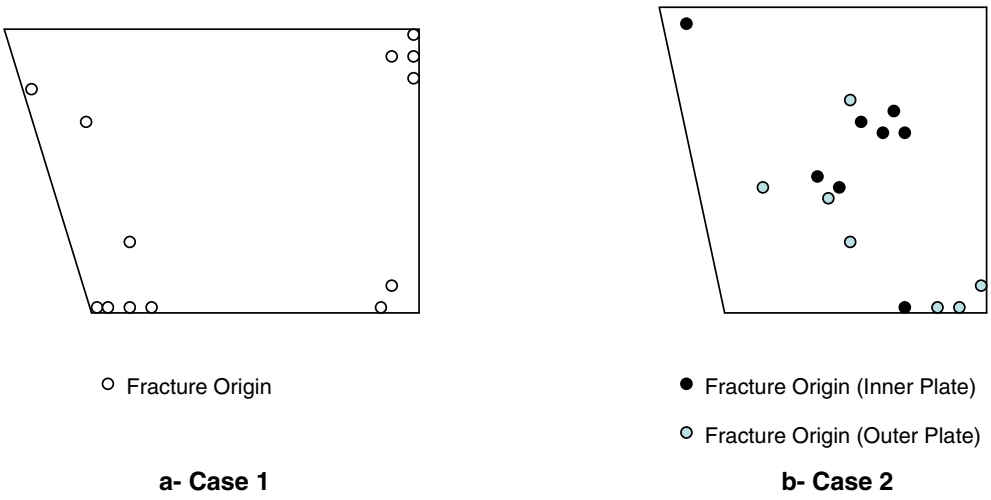

Figure 7 Fracture origins for test specimens.

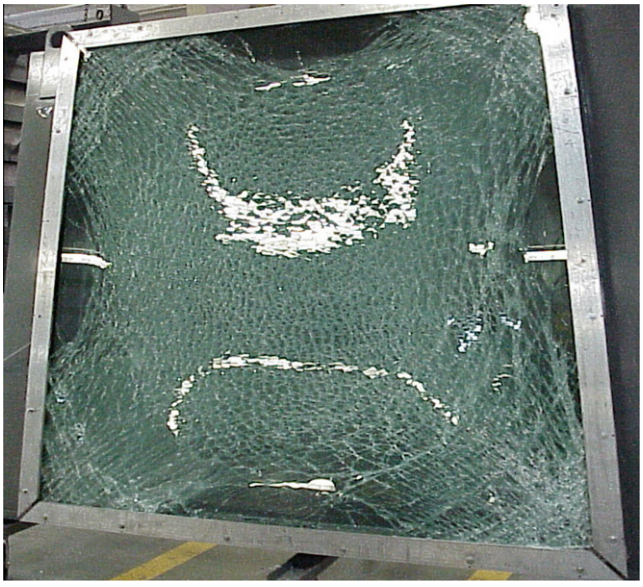

Figure 8 Fracture pattern for laminated specimen.

Fig. 3). Steel channels with 152 mm depth were welded together to form the support of the specimen. These channels in turn are welded to a 12 mm base plate. To simulate the wind pressure on the experimental a vacuum machine was used to exhaust the air from inside the chamber. This machine consists of vacuum tanks, and a control panel which contains a valve system and the vacuum supply as seen in Fig. 2.

The models of the glazing system described earlier are used to analyze several examples. The following data were employed:

Modulus of elasticity for glass, E	10^7 psi (68.9 GPa)
Shear modulus for PVB	145 psi (1 MPa)
Thickness of monolithic plate	3/8 in. (10 mm)
Thickness of LG plate	1.5 in. (38 mm)
Interlayer thickness (PVB)	0.09 in. (2.29 mm)
Poisson's ratio, v	0.22
Design load for monolithic plate	0.293 psi (2.02 kPa)
Design load for LG plate	2.21 psi (15.2 kPa)

It should be noted that the boundary conditions are simply supported for all the experimental and numerical examples.

3.1. Example 1

The example involves two typical plates with overall dimension as shown in Fig. 4. As seen in Fig. 5, the experimental vertical displacements at the center of the model were compared with the results of the FEM Case 2. At each point, the experimental results were repeated several times and one theoretical result was calculated using FEM for a particular pressure. It can be seen from Fig. 5 that if the average of the experimental results is taken, it matches very well with the FEM results.

The resulting stresses in the glass plates are transformed to obtain principal stresses and are shown in Fig. 6. It should be noted that the principal stresses are computed only for glass plate in the tension side of the LG. The maximum values of tensile principal stresses are 3496 psi (24.1 MPa) and 3477 psi (23.97 MPa) for monolithic plates and LG plate, respectively, and located at corner **O**. It can be seen from the stress contours in Fig. 6 that the stresses in the other corners and at the center are very close to the maximum value at **O**. The fracture origins for test specimens and an example of fractured specimen after the test are shown in Figs. 7 and 8, respectively.

The comparison of fracture origins from experimental data (Fig. 7) shows an excellent match with locations of the highest tensile principal stresses, as shown in Fig. 6.

3.2. Example 2

In this example, the FEM was applied to example 1 except that the angle ϕ is 90°, as seen in Fig. 1. Then, the same procedure was used by moving point **O** towards point **O′** to create two triangles with angles $\phi = 37.93°$ and 45° for Case 1 and Case 2, respectively (Fig. 4). Also, the FEM was employed to solve two hexagonal monolithic and LG plates shown in Fig. 9. The maximum tensile principal stresses contours are shown in Figs. 10–12 for rectangular, triangular, and hexagonal shapes, respectively. The dimensions of the rectangular shape are chosen to bound the other shapes as shown in Fig. 4. Due to

symmetry, only one-quarter of the plate is presented in both rectangular and hexagonal shapes. The maximum values of principal stresses for rectangular shape are 3110.0 psi (21.44 MPa) and 3494.0 psi (24.1 MPa) for monolithic and LG plates, respectively, as shown in Fig. 10. The location of the highest stresses in monolithic glass plate occurs at the corner, but for the LG plate it occurs at the center. Fig. 10 shows that the value at the corner is very close to the highest one for LG. Previous studies [5,13] have indicated that the maximum principal stress will be at the corner of rectangular LG plates. This example shows that the load with respect to the total thickness is small to produce nonlinearity and as the load is increasing, the location of the highest stresses will move gradually to the corner of the plate.

In Fig. 11, the maximum values of principal stress for triangular glass plates are 2414.0 psi (16.65 MPa) and 1932.85 psi (13.32 MPa) for monolithic and LG plates, respectively. The locations of maximum principal stresses move to the center of the plate, as shown in the figure. For the hexagonal shapes, the location of maximum principal stresses are at the corner A with values of 4756.89 psi (32.8 MPa) and 4020.0 psi (27.72 MPa) for monolithic and LG plates, respectively, as shown in Fig. 12. Tables 1 and 2 summarize the relative maximum values of principal stress obtained from the

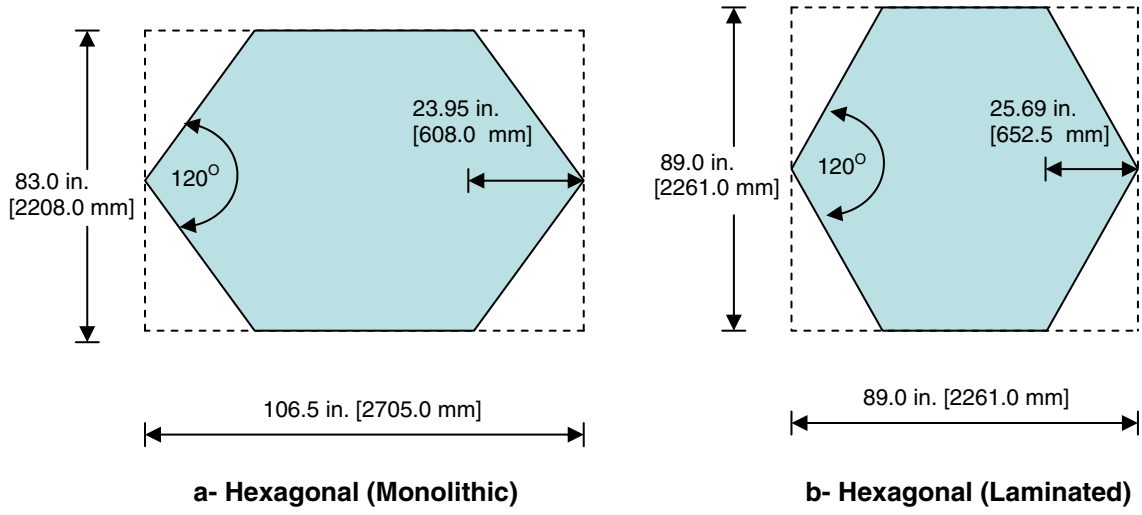

Figure 9 Overall dimension of hexagonal shapes.

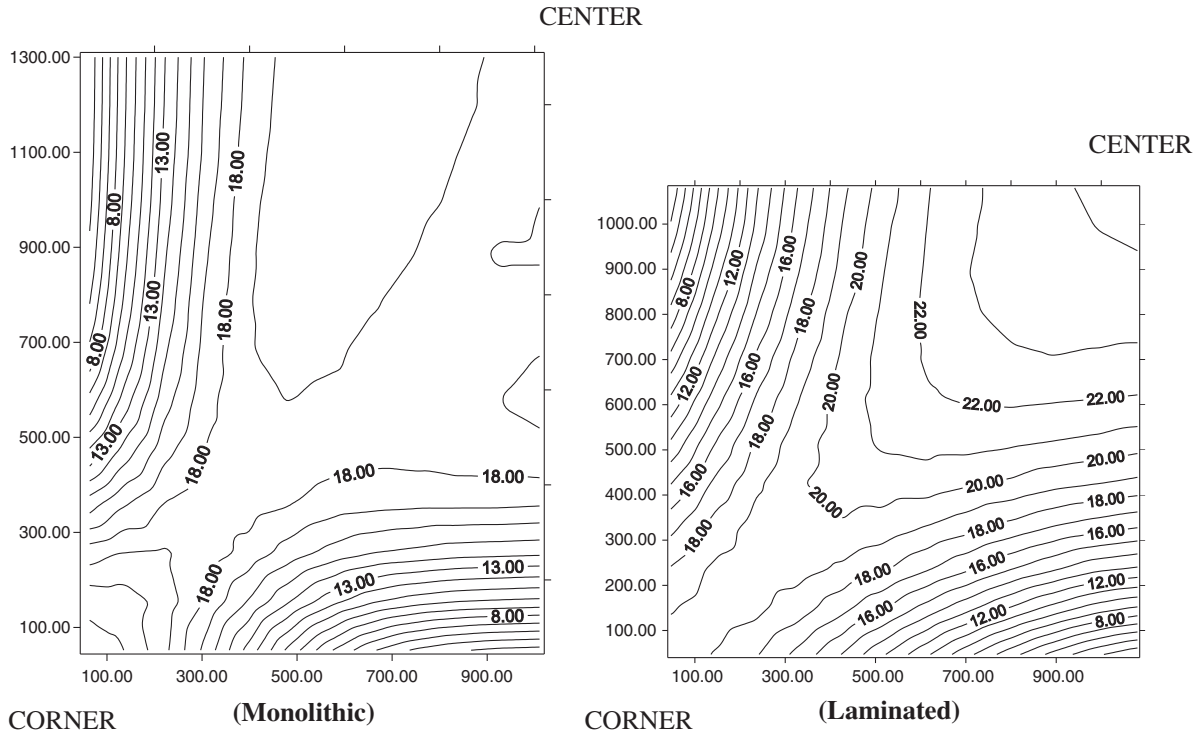

Figure 10 Maximum tensile principal stresses (rectangular shape) (stress contours in MPa; dimensions on axes in mm).

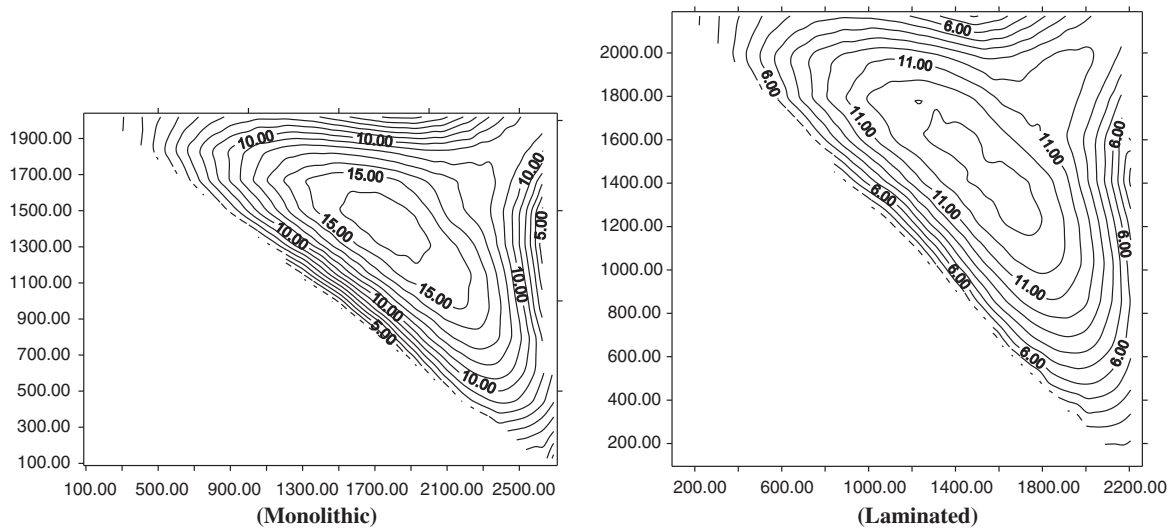

Figure 11 Maximum tensile principal stresses (triangular shape) (stress contours in MPa; dimensions on axes in mm).

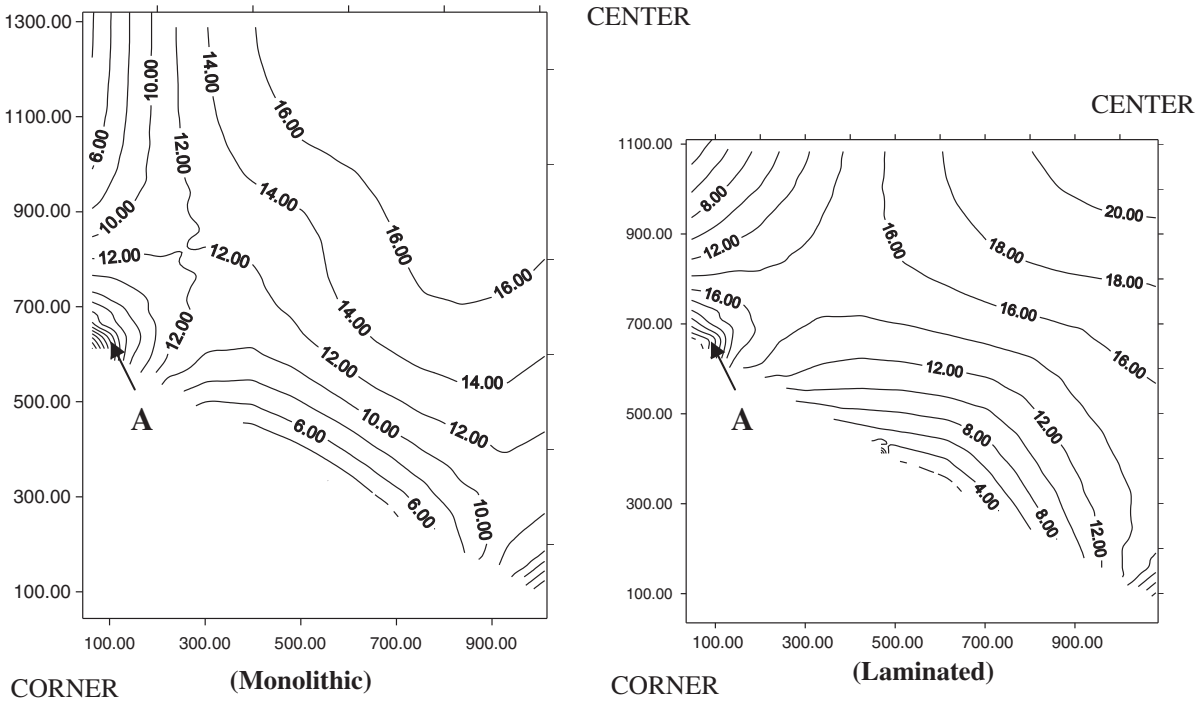

Figure 12 Maximum tensile principal stresses (hexagonal shape) (stress contours in MPa; dimensions on axes in mm).

rectangular, triangular, trapezoidal and hexagonal plates for monolithic and LG plates. These values are normalized w.r.t. the maximum principal stress obtained from the rectangular plate.

3.3. Example 3

In this example, a circular plate is considered with the following dimensions:

Plate diameter is 2.0 m.
Thickness of PVB interlayer = 0.38 mm.
Total thickness of the glass plate = $t_1 + t_2$, where $t_1 = t_2 = 5$, 7.5 and 10 mm.
Modulus of elasticity of glass (E) = 68.9 GPa.
Poisson's ratio of glass = 0.22.
Shear modulus of PVB interlayer (G_{INT}) = 689.5 kPa.

Fig. 13 shows the finite element mesh used for 1/4 of the plate. The maximum non-dimensional displacements (w/t) at the center of the plate are plotted versus pressure in Fig. 14 showing that geometric nonlinearity occurred for LG circular plates. The figure also shows that as the thickness of the plate increased the nonlinearity decreased. This can be attributed to

Table 1 Value of maximum principal stress normalized w.r.t. that of the rectangular plate for monolithic plates.

Plate shape	Max. stress value
Rectangular	1.00
Triangular	0.62
Trapezoidal	1.13
Hexagonal	1.53

Table 2 Value of maximum principal stress normalized w.r.t. that of the rectangular plate for LG plates.

Plate shape	Max. stress value
Rectangular	1.00
Triangular	0.70
Trapezoidal	1.00
Hexagonal	1.15

the effect of shear deformation on the nonlinear solutions as a result of using Mindlin plate elements. The maximum principal stresses along the radius of the plate for both bottom and top plates are plotted in Figs. 15 and 16, respectively, for thicknesses $t_1 = t_2 = 5$ mm for several pressures. The pressure values of load 1 to load 6 are 21.55, 43.1, 64.65, 86.2, 107.75 and 128.1 kPa, respectively. It can be seen, from Fig. 15, that the maximum principal stresses are changing from tension to compression along the radius of the plate under high pressures (load 4 to load 6). Meanwhile, the maximum principal stresses at the top of the plate remain in tension. It can be shown from these results that nonlinear analysis should be considered in circular LG plates. The present finite element model covers effectively the behavior of circular glass plates with simple formulation for the interlayer material.

For the given examples, the maximum values of (w/t) are 2.5 for example 1 and 6.4, 2.15 and 0.9 for example 2 for $t_1 = t_2 = 5$, 7.5 and 10 mm, respectively. According to ASTM 1300-09a [1], the corresponding maximum values of (w/t) for the same thicknesses are 5, 5.5, 4 and 3 for both examples, which ensures that the results agree with the limitations of ASTM 1300-09a [1] except the first value of example 2. This value $(w/t = 6.4)$ is higher than the limitations with 16% and associated with the smaller thickness (10 mm). Also, it should be noted that with these high values of (w/t), the material still behaves within the elastic region since the glass is brittle material. Table 3 shows the maximum values of non-dimensional displacements, w/t, obtained from the circular plate, along with the limitations of ASTM 1300-09a [1].

4. Summary and conclusion

High order finite element computer models have been used to analyze several examples with trapezoidal, rectangular, triangular, and hexagonal shaped glass plates. Both monolithic and LG cases were studied. The computed data were compared with the experimental data for trapezoidal shapes. The following conclusions are drawn from this study:

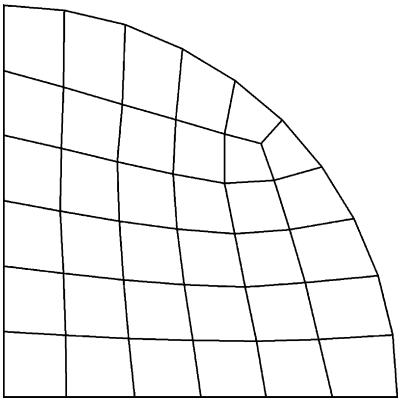

Figure 13 Finite elements mesh for 1/4 of a circular plate.

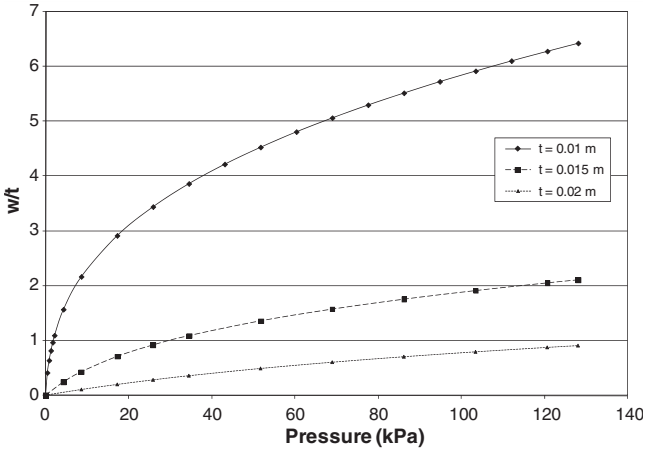

Figure 14 Maximum non-dimensional deflection versus pressure.

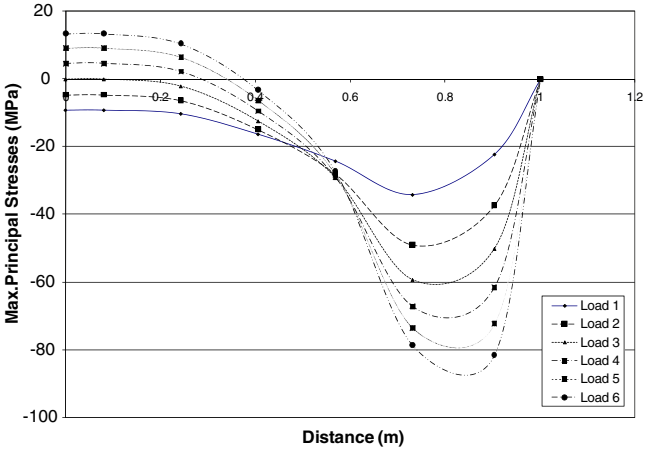

Figure 15 Maximum principal stresses at the bottom plate.

1. The comparison between the results of the finite element model and the results of the experiments on both monolithic and LG plates is very good. This demonstrates the capability of the finite element model to handle these problems.

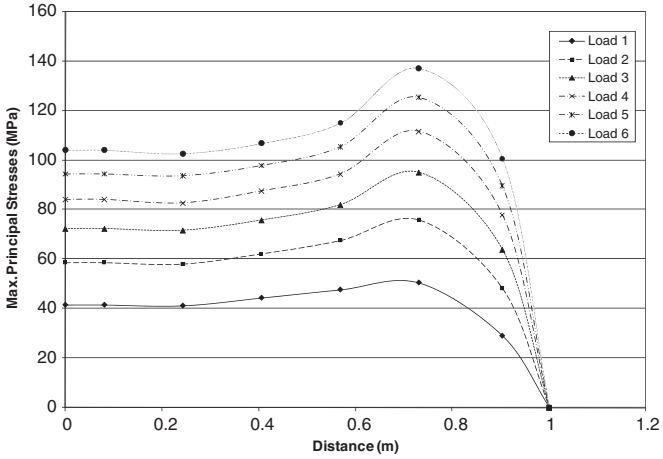

Figure 16 Maximum principal stresses at the top plate.

Table 3 Comparison between results of the circular plate and ASTM 1300-09a limitations.

Total thickness of glass plate (mm)	Maximum non-dimensional displacements (w/t)	Limitations of ASTM
10	6.4	5.50
15	2.15	4.00
20	0.9	3.00

2. In trapezoidal monolithic glass plates, the maximum principal tensile stress is approximately 13% higher than that in the bounding rectangular shapes. For LG, the maximum principal tensile stresses are almost the same in trapezoidal shapes and their bounding rectangular shapes.
3. For triangular shapes, the values of maximum tensile principal stresses are 62% and 70% of rectangular shapes for monolithic and LG plates, respectively.
4. For hexagonal shapes, the ratios of maximum principal tensile stresses with respect to the bounding rectangle are 1.53 and 1.15 for monolithic and LG plates, respectively.
5. The basis of window glass design is not the maximum principal tensile stress, but rather the probability of breakage. Consequently, to obtain a more complete understanding, results of the FEM analysis must be coupled with failure prediction methodology [2,10] to obtain a complete picture.
6. The capability of the present finite element model to handle circular LG plates without transformation of axes from rectangular to polar axes.
7. Circular LG plates are producing geometric nonlinearity especially for small thickness, and as the thickness increased the nonlinearity decreased.
8. Under high pressure, the maximum principal stresses are changing in sign at the compression side of the plate depending on the load direction. This conclusion is very important to be considered in the design of such kind of plates.
9. In order to get good results for nonlinearity in LG plates, a suitable number of elements should be applied with small load increments.

Acknowledgements

The material presented here is based on research work performed at the Glass Research and Testing Laboratory (GRTL), Department of Civil and Environmental Engineering, Texas Tech University, Lubbock, TX, US.

The authors wish to thank Dr. H. Scott Norville, Director of GRTL, Texas Tech University, Lubbock, TX, for his encouragement and support during the course of this research.

References

[1] ASTM, Standard Practice for Determining the Minimum Thickness and Type of Glass Required to Resist A Specified Load, 2009 Annual Book of ASTM Standards, Standards E 1300-09, Philadelphia, US, 2009.
[2] W.L. Beason, A Failure Prediction Model for Window Glass, NTIS Accession No. PB81-148421, Institute for Disaster Research, Texas Tech University, Lubbock, TX, 1980.
[3] R.D. Cook, D.S. Malkus, M.E. Plesha, Concepts and Applications of Finite Element Analysis, John Wiley & Sons, New York, 1989.
[4] M.M. El-Shami, K.S. Kandil, M. Abdel Haliem, Experimental behavior of triangular laminated glass plates, in: Proceedings of the Building Integration Solutions, Architectural Engineering 2008 Conference, ASCE, Denver, CO, 2008, pp. 24–27.
[5] M.M. El-Shami, H.S. Norville, Finite element modeling of architectural laminated glass, IES Journal Part A: Civil and Structural Engineering 4 (1) (2011).
[6] M.M. El-Shami, C.V.G. Vallabhan, S.A. Kandil, Comparison of nonlinear Von Karman and Mindlin plate solutions, in: Proceedings of the Texas ASCE Conference, American Society of Civil Engineers, Texas Section, Spring Meeting, Houston, TX, 1997, pp. 401–408.
[7] R. Kaiser, Rechnerische und experimentelle ermittlung der durchbiegungen und spannungen von quadratischen platten bei freier auflagerung an den randern, Gleichmassig verteilter Last und grossen Ausbeigungen, Z. f. a. M. M., Bd. 16, Heft 2, 1936, pp. 73–98.
[8] S. Levy, Bending of Rectangular Plates with Large Deflection, NACA, Technical Note No. 846, 1942.

[9] H.S. Norville, K.W. King, J.L. Swofford, Behavior and strength of laminated glass, Journal of Engineering Mechanics, ASCE 124 (1) (1998) 46–53.
[10] H.S. Norville, J. Minor, The strength of weather window glass, American Ceramic Society Bulletin 64 (11) (1984).
[11] A.C.I. Pilkington, A Practical and Theoretical Investigation into the Strength of Laminated Glasses under Uniformly Distributed Loading, Laboratory Report and Discussion, Pilkington ACI Operations Pty. Ltd., Dandenong, 1971, p. 206.
[12] C.V.G. Vallabhan, Iterative analysis of nonlinear glass plates, Journal of Structural Engineering, ASCE 109 (2) (1983) 489–502.
[13] C.V.G. Vallabhan, Y.C. Das, M. Magdi, M. Asik, J.R. Bailey, Analysis of laminated glass units, Journal of Structural Engineering, ASCE 119 (5) (1993) 1572–1585.
[14] C.V.G. Vallabhan, M.M. El-Shami, Comparison of rectangular glass plates with area-equivalent trapezoidal plates, in: Proceedings of the American Society of Civil Engineers, Texas Section, Spring Meeting, San Antonio, TX, March 2001, pp. 267–274.
[15] Th. von Karman, Festigkeitspobleme in maschinenbau, Encyk. Der Math. Wiss., vol. IV, 1910, p. 349.
[16] O.C. Zienkiewicz, The Finite Element Method, McGraw-Hill, London, 1977.